

AD-L-JEPA: Self-Supervised Spatial World Models with Joint Embedding Predictive Architecture for Autonomous Driving with LiDAR Data

Haoran Zhu^{*,1}, Zhenyuan Dong^{**1}, Kristi Topolai^{**1}, Anna Choromanska¹

Abstract—As opposed to human drivers, current autonomous driving systems still require vast amounts of labeled data to train. Recently, *world models* have been proposed to simultaneously enhance autonomous driving capabilities by improving the way these systems understand complex real-world environments and reduce their data demands via self-supervised pre-training. In this paper, we present AD-L-JEPA (aka Autonomous Driving with LiDAR data via a Joint Embedding Predictive Architecture), a novel self-supervised pre-training framework for autonomous driving with LiDAR data that, as opposed to existing methods, is neither generative nor contrastive. Our method learns spatial world models with a joint embedding predictive architecture. Instead of explicitly generating masked unknown regions, our self-supervised world models predict Bird’s Eye View (BEV) embeddings to represent the diverse nature of autonomous driving scenes. Our approach furthermore eliminates the need to manually create positive and negative pairs, as is the case in contrastive learning. AD-L-JEPA leads to simpler implementation and enhanced learned representations. We qualitatively and quantitatively demonstrate high-quality of embeddings learned with AD-L-JEPA. We furthermore evaluate the accuracy and label efficiency of AD-L-JEPA on popular downstream tasks such as LiDAR 3D object detection and associated transfer learning. Notably, our method achieves up to a $5\times$ speed-up in pre-training time compared with the state-of-the-art (SOTA) approaches and consistently delivers better performance when fine-tuned on different amounts of labeled data compared to SOTA. More impressively, the experiments show that even when the first layers of the encoders of AD-L-JEPA are randomly initialized while the remaining layers are initialized as pre-trained, our method still yields positive transfers, whereas the competitor method suffer from the negative transfers in this case. Systematic experimental results demonstrate that our method learns a robust spatial world model in the BEV embedding space, resulting in faster pre-training times, improved generalization, and enhanced label efficiency. Our experimental evaluation demonstrates that AD-L-JEPA is a plausible approach for self-supervised pre-training in autonomous driving applications and is the best available approach outperforming SOTA, including most recently proposed Occupancy-MAE [1] and ALSO [2]. The source code of AD-L-JEPA is available at <https://github.com/HaoranZhuExplorer/AD-L-JEPA-Release>.

I. INTRODUCTION

LiDAR data is one of the most common data modalities in autonomous driving. Existing autonomous driving systems need to collect vast amounts of raw LiDAR data

¹Learning Systems Laboratory, Department of Electrical and Computer Engineering, New York University, 370 Jay Street, NY, USA. {hz1922, zd2362, kt2664, ac5455}@nyu.edu

*Main contributor.

**Equal contribution.

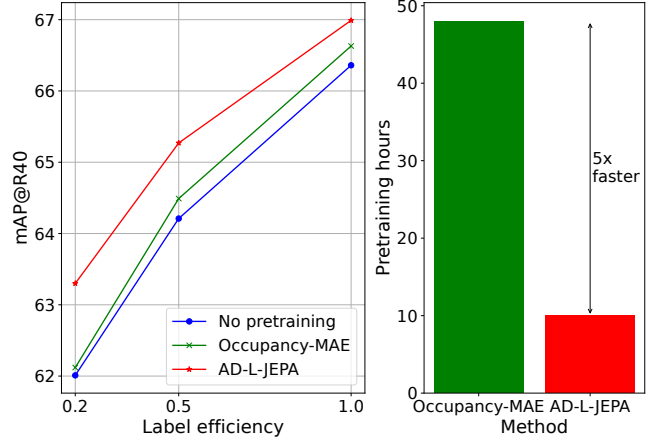


Fig. 1: AD-L-JEPA consistently improves label efficiency when transferring from the Waymo (subsamped 20% of the data set is used) to the KITTI3D data set in the LiDAR object detection task (we use SECOND [3] detection model), and achieves a $5\times$ speed-up in pre-training time.

across various driving scenarios and then annotate them with labels, which is expensive, time-consuming, and limits the scalability. And in particular, label annotation constitutes a significant bottleneck here since the collection of unlabeled data alone is much easier. Recently, researchers have proposed to have a common backbone for different learning tasks that is pre-trained in a self-supervised manner without any labels and then only fine-tune the whole network with labeled data [1], [2] to adapt to specific downstream tasks. This approach requires less labeled data and is therefore more practical.

A key to further enhancing autonomous driving capabilities may therefore lie in learning self-supervised world models [4] as a novel pre-training paradigm. Furthermore, learning world models in a self-supervised manner enables the network to predict unknown states of the environment, which helps to manage uncertainty in the autonomous driving systems.

What is our contribution and what makes us different from SOTA? In this paper, we propose a novel self-supervised pre-training method **AD-L-JEPA** for LiDAR data. To the best of our knowledge, this is the first JEPA-based pre-training framework for autonomous driving. Our method learns a self-supervised spatial world model in Bird’s Eye View (BEV) space and predicts embeddings for spatially unknown regions. Since it predicts BEV embeddings, instead

of explicitly reconstructing the unknown parts of the data, it *improves the quality of the data modeling* (embeddings contain the most relevant information, including relevant details, for example a car hidden behind the truck may not show in reconstructed data but still can be well captured in BEV embeddings) and allows to *better adapt to the data uncertainty*, which leads to *better generalization*. It is also extremely *efficient* and *significantly reduces the pre-training time*. Furthermore, AD-L-JEPA learns *high-quality embeddings*, which also results in *superior label efficiency on downstream tasks*. Motivating illustration demonstrating the advantages of AD-L-JEPA is captured in Figure 1. The implementation of AD-L-JEPA is straightforward and omits the necessity to create human-crafted positive/negative pairs, as is the case in contrastive learning. Finally, AD-L-JEPA adds to the existing family of self-supervised pre-training methods for autonomous driving applications a new approach that *compares favorably to the existing SOTA, including most recently proposed Occupancy-MAE [1] and ALSO [2]*. The source code of AD-L-JEPA is released.

II. BACKGROUND AND RELATED WORKS

A. Self-supervised learning

Self-supervised learning aims at learning useful data representations from the unlabeled data. We focus here on self-supervised learning approaches that are dedicated to autonomous driving with LiDAR point cloud data. Among the existing methods, contrastive techniques learn self-supervised representations by maximizing the feature similarity of manually created positive pairs (matching points) from different levels, such as point level [5], depth map level [6], region clusters level [7], spatial or temporal segments [8], [9], [10], [11], [12], [13], [14], [15], or Bird’s Eye View (BEV) features over time [16], while minimizing the similarity of negative pairs (non-matched points), if any. Another family of approaches are the generative-based method, where the network is trained to reconstruct masked point clouds [1], [17], [18], [14] or scene surfaces [2], [19].

Besides contrastive and generative methods, another novel self-supervised learning paradigm offers joint-embedding predictive architecture (JEPA). It has recently been applied to image and video data modalities [4], [20], [21] but has not yet been explored for autonomous driving scenarios. JEPA learns meaningful representations by predicting the embeddings of the unknown parts of data extracted by a target encoder given the known parts embeddings extracted by a context encoder. Unlike contrastive learning, it does not require complicated pre-processing to create positive pairs and does not suffer from the curse of dimensionality with negative pairs (these are the commonly-known drawbacks of contrastive learning [4]). Furthermore, it effectively captures the high uncertainty of the environment without explicitly generating reconstructions of unknown regions that is typically done by generative methods. Our proposed AD-L-JEPA is the first JEPA-based pre-training method dedicated for autonomous driving.

Representation collapse is a common phenomenon, when the network fails to learn meaningful representations. It can manifest in two ways: complete collapse, where all representations reduce to a constant vector and thus become useless, or dimensional collapse, where the dimensions of learned representations are highly correlated with each other and contain redundant information. Generative-based methods naturally avoid complete collapse when the dimension of the information bottleneck in the encoder is smaller than the dimension of the input, as generating unknown regions requires learning meaningful representations. Contrastive-based methods avoid complete collapse by creating contrastive pairs to learn distinctive representations. For JEPA-based methods, regularization techniques and moving average updates of the target encoder have been proven useful [22], [20], [21]. There are also studies that quantitatively measure the degree of representation collapse by examining the singular value spectrum of the learned representations [23]. In our paper, we employ both regularization techniques and moving average updates of the target encoder to prevent collapse.

B. World models for autonomous driving

World Models [24], [4], [25] aim at modeling the possible spatially unknown states or future states of the environment to help the agent navigate in it. World models help understanding the data and model uncertainties in the data. Instead of explicitly predicting data in pixel space, the method based on the joint-embedding predictive architecture [20] proposes predicting embeddings of masked or future image patches in a self-supervised manner [21] to capture multiple potential states. Also, given a context video or text, world models allow to generate possible future videos. In autonomous driving scenarios, world models have been deployed as a data engine [26], to mitigate covariance shift [27], to improve end-to-end driving [28], [29], and for pre-training [30].

C. LiDAR-based 3D object detection

We use 3D Object Detection as the downstream task to evaluate the effectiveness of our pre-training method for autonomous driving with LiDAR data. For most LiDAR-based 3D object detection downstream algorithms, a sparse 3D convolution encoder first extracts 3D voxel representations from a given point cloud scene. It then reshapes the image over the height dimension and applies 2D dense convolutions to generate BEV representations. Finally, either a single-stage [3] or a two-stage detection head [31], [32], [33] is attached for the LiDAR-based 3D object detection task. Following common settings in the literature, we focus on conducting self-supervised pre-training and evaluate the pre-trained feature quality also using the sparse 3D convolution encoder framework.

III. METHOD

The architecture of AD-L-JEPA is shown in Figure 2. The overarching intuition behind our framework is as follows: for the visible parts of the point cloud scene, the network is

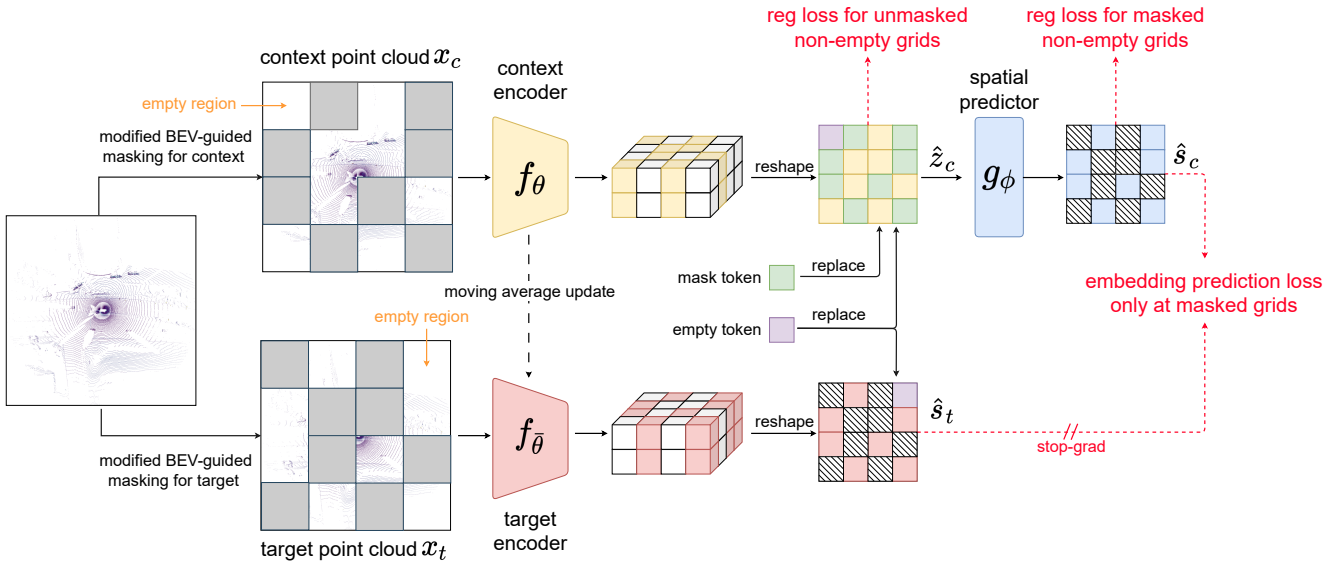


Fig. 2: The overview of AD-L-JEPA architecture.

trained in a self-supervised manner to predict how the invisible parts should appear in the embedding space. This enables the learning of geometrically and semantically reasonable world models, as well as adapting to the high uncertainty nature of the autonomous driving scenes by avoiding the explicit reconstruction of the invisible parts of the data.

In the following subsections we describe our design in detail. First, we mask the input point cloud with our proposed modified BEV-guided masking (Section III-A). Next, unmasked points are sent to the context encoder, and masked points are sent to the target encoder (Section III-B). We then replace the empty regions in both context and target BEV embeddings with a learnable empty token, and the masked regions in the context BEV embedding with a learnable masked token (Section III-C). Later, a lightweight predictor predicts target BEV embeddings from context BEV embeddings (Section III-D). Finally, we train the context encoder and predictor using cosine similarity-based embedding prediction loss and variance regularization loss, while we update the target encoder through a moving average strategy. This ensures the learning of high-quality, non-collapsed representations (Section III-E).

A. Modified BEV-guided masking

To learn effective spatial world models in a self-supervised manner, masking is used to create invisible and visible regions. The network is then trained to predict embeddings of the invisible regions based on the visible ones. We have two design recipes for masking in autonomous driving scenarios: (1) masks are first created in the BEV embedding space and recursively upsampled to the input point cloud to identify points to be masked; (2) both empty and non-empty areas should be included in the visible and invisible regions created by the masks. These two criteria can be achieved by modifying the BEV-guided masking originally proposed in [17] (see comparison in Figure 3).

The original BEV-guided masking involves projecting points onto non-overlapping BEV grids, creating masks only

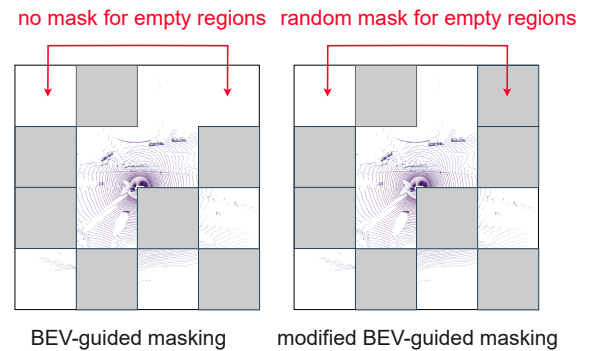


Fig. 3: Comparison of original BEV-guided masking [17] with our modified version that creates masks in both empty and non-empty regions in non-overlapping BEV grids.

in non-empty BEV grids, and reconstructing only in the masked non-empty regions. This assumes that the network already knows which BEV grid is empty, which stands in contrast with our goal to learn a spatial world model to predict all invisible regions. As opposed to this approach, we create masks for both empty and non-empty BEV grids, resulting in visible and invisible parts that contain both empty and non-empty regions. Consequently, the network is trained to predict the embeddings of all invisible parts, including those that contain empty regions, which enhances the encoder’s representation power and helps to learn good quality spatial world models. In our experiments, masks are applied to 50% of non-empty BEV grids and 50% of empty BEV grids. The input points sent to the encoder remain the same as in the original BEV-guided masking. However, the encoder’s output BEV embeddings will later be replaced by mask tokens for both masked empty and non-empty grids, whereas in [17], only masked non-empty grids were replaced by mask tokens. We denote the unmasked point cloud as $\mathbf{x}_c = \{\mathbf{x}_c^1, \dots, \mathbf{x}_c^N\}$ and the masked point cloud as $\mathbf{x}_t = \{\mathbf{x}_t^1, \dots, \mathbf{x}_t^N\}$ in the multi-batch setting with a batch size of N . \mathbf{x}_c and \mathbf{x}_t are then sent to the context encoder

and target encoder, respectively.

B. Context encoder & target encoder

The context encoder f_θ and target encoder $f_{\bar{\theta}}$ are backbones responsible for extracting context embeddings from the unmasked point cloud and target embeddings from the masked point cloud, respectively. The context encoder will later be used for fine-tuning on the downstream tasks after self-supervised representation learning. It receives input point cloud features and outputs embeddings in a down-sampled 3D space $\in \mathbb{R}^{N \times H \times W \times D \times C}$, where H , W , and D represent the length, width, and height dimensions of the 3D embedding, and C is the embedding dimension. We obtain BEV embeddings by reshaping the 3D embeddings. The context BEV embedding is denoted as $\mathbf{z}_c = \text{reshape}(f_\theta(\mathbf{x}_c)) \in \mathbb{R}^{N \times H \times W \times D \times C}$, and the target BEV embeddings as $\mathbf{s}_t = \text{reshape}(f_{\bar{\theta}}(\mathbf{x}_t)) \in \mathbb{R}^{N \times H \times W \times D \times C}$.

C. Learnable empty token and mask token

We introduce a learnable empty token ($\in \mathbb{R}^{D \cdot C}$) and a learnable mask token ($\in \mathbb{R}^{D \cdot C}$). By forwarding the unmasked point cloud to the context encoders and the masked point cloud to the target encoders, and after reshaping, we replace all unmasked empty grids in \mathbf{z}_c and \mathbf{s}_t with the learnable empty token. Simultaneously, we replace all masked grids in \mathbf{z}_c with the learnable mask token. We then apply L_2 normalization to each BEV grid’s embedding dimension. We denote the context embeddings and target embeddings after such a process by $\hat{\mathbf{z}}_c \in \mathbb{R}^{N \times H \times W \times D \cdot C}$ and $\hat{\mathbf{s}}_t \in \mathbb{R}^{N \times H \times W \times D \cdot C}$, respectively.

D. Predictor

The predictor is a lightweight, three-layer convolutional network g_ϕ that predicts target BEV embeddings from visible context BEV embeddings. We denote the predicted embedding, after the L_2 normalization is applied to each BEV grid’s embedding dimension, as $\hat{\mathbf{s}}_c = g_\phi(\hat{\mathbf{z}}_c)$, where $\hat{\mathbf{s}}_c$ is in $\mathbb{R}^{N \times H \times W \times D \cdot C}$ and has the same shape as the target BEV embeddings.

E. Training

We pre-train the network in a self-supervised manner with two losses to ensure we learn high-quality, non-collapsed embeddings: a cosine similarity-based embedding prediction loss and a variance regularization loss.

For predicted embeddings $\hat{\mathbf{s}}_c$, we are primarily concerned with the embeddings of masked BEV grids, as we already know the embedding of unmasked BEV grids. Thus, we minimize the cosine similarity-based embedding prediction loss only for the masked grids. We also notice that objects in autonomous driving scenarios are distributed in a sparse manner; the number of BEV grids mapped with no points (empty grids) is significantly larger than the number of BEV grids mapped with points (non-empty grids). Therefore, we introduce the hyperparameters $\alpha_0 = 0.25$ and $\alpha_1 = 0.75$ to balance the loss. Overall, the prediction loss is:

$$\mathcal{L}_{\text{jepa}} = \frac{\alpha_0}{\sum_{n=1}^N |P_n|} \sum_{n=1}^N \sum_{i=1}^{|P_n|} \left(1 - \frac{\hat{\mathbf{s}}_c^n[i] \cdot \hat{\mathbf{s}}_t^n[i]}{\|\hat{\mathbf{s}}_c^n[i]\| \|\hat{\mathbf{s}}_t^n[i]\|} \right) + \frac{\alpha_1}{\sum_{n=1}^N |Q_n|} \sum_{n=1}^N \sum_{j=1}^{|Q_n|} \left(1 - \frac{\hat{\mathbf{s}}_c^n[j] \cdot \hat{\mathbf{s}}_t^n[j]}{\|\hat{\mathbf{s}}_c^n[j]\| \|\hat{\mathbf{s}}_t^n[j]\|} \right), \quad (1)$$

where P_n is the subset containing all indices of unmasked empty BEV grids, and Q_n is the subset containing all indices of unmasked non-empty BEV grids in the n -th input in a multi-batch setting. We also denote K_n as the subset containing all indices of masked non-empty BEV grids in the n -th input.

In order to avoid representation collapse, we apply an additional variance regularization loss proposed by [22]:

$$\mathcal{L}_{\text{reg}} = \beta_1 \sum_{n=1}^N v(\hat{\mathbf{z}}_c^n[K_n]) + \beta_2 \sum_{n=1}^N v(\hat{\mathbf{s}}_c^n[Q_n]), \quad (2)$$

where the function $v(\cdot)$, which uses an arbitrary input 2D embedding matrix $Y \in \mathbb{R}^{M \times C}$ recording an arbitrary number M of embeddings with a fixed embedding dimension C , is defined in [22]:

$$v(Y) = \frac{1}{C} \sum_{j=1}^C \max(0, \gamma - \sqrt{\text{Var}(Y^j) + \epsilon}). \quad (3)$$

This loss ensures that the average variance across all embedding dimensions, for all unmasked non-empty grids’ BEV embeddings after the context encoder $\hat{\mathbf{z}}_c^n[K_n] \in \mathbb{R}^{|K_n| \times C}$, and all masked non-empty grids’ BEV embeddings after the predictor $\hat{\mathbf{s}}_c^n[Q_n] \in \mathbb{R}^{|Q_n| \times C}$, is larger than some threshold γ . This approach prevents the learning of a meaningless constant embedding. Note that the regularization loss must be computed across each input in the multi-batch setting; otherwise, as we empirically observe, the network tends to learn another meaningless solution consisting of N constant embeddings. These embeddings are significantly distinct from each other and are assigned to all non-empty grids in the n -th input, respectively. In this scenario, although the overall variance exceeds the threshold γ , each BEV embedding in the n -th input remains constant, which is meaningless. Averaging the loss across each input helps avoid this issue.

The overall self-supervised learning loss is:

$$\mathcal{L} = \lambda_{\text{jepa}} \mathcal{L}_{\text{jepa}} + \lambda_{\text{reg}} \mathcal{L}_{\text{reg}} \quad (4)$$

The parameters of the context encoder, the predictor, as well as the learnable mask token and the learnable empty token, are all updated by gradient descent using Equation 4. Meanwhile, the parameters of the target encoder are updated through a moving average of the context encoder’s parameters, $\phi \leftarrow \eta \phi + (1 - \eta)\theta$, to further avoid representation collapse, as proposed in [20], [21].

IV. EXPERIMENTS

To evaluate our pre-training method relying on self-supervised spatial world models, we use a LiDAR 3D object detection task as a downstream fine-tuning task. We utilize the OpenPCDet framework [34] to pre-process the data sets and conduct the experiments.

A. Data sets

We use KITTI3D [35] and Waymo [36] data sets to conduct self-supervised pre-training and downstream fine-tuning. The KITTI3D data set contains a total of 3712 training frames and 3769 validation frames. We report the 3D object detection Average Precision (AP) metric, calculated at 40 recall positions (R_{40}) and 11 recall positions (R_{11}), for the moderate level of difficulty¹ across different classes on KITTI3D data set. The Waymo data set contains a total of 158081 training frames and 39987 validation frames. Following the popular setting of OpenPCDet, we subsample 20% of the training frames with a sampling interval of 5, resulting in 31617 training frames. We report the 3D object detection Average Precision (AP) metric and Average Precision with Heading (APH) metric for LEVEL 2 difficulty across different classes on Waymo data set.

B. Network settings

We use our proposed AD-L-JEPA to pre-train the popular VoxelBackBone8x encoder, which contains 12 sparse convolution layers. For both the KITTI3D and 20% subsampled Waymo data sets, we pre-train the network with unlabeled training data only for 30 epochs using the Adam optimizer and the default one-cycle learning rate scheduler in OpenPCDet, with a learning rate of 0.0003 and a weight decay of 0.01. We set the initial η to 0.996 and increase it linearly to 1, following [21], for the moving average update. We set masking ratio = 0.5. We set $\alpha_0 = 0.25$ and $\alpha_1 = 0.75$ for empty grids and non-empty, respectively. We set $\beta_1 = 1$ and $\beta_2 = 1$. The threshold for variance regularization, γ , is set to $\frac{1}{\sqrt{D}} = \frac{1}{16}$ for L_2 -normalized embeddings. For the KITTI3D data set, the shape for BEV embedding is $H = 200$, $W = 176$, $D = 2$, $C = 128$; we set $\lambda_{\text{jepa}} = 1$ and $\lambda_{\text{reg}} = 1$ to balance the two loss functions. For the Waymo data set, the shape for BEV embedding is $H = 188$, $W = 188$, $D = 2$, $C = 128$; we set $\lambda_{\text{jepa}} = 1$ and $\lambda_{\text{reg}} = 10$ to balance the two loss functions. We use 4 1080 Ti GPUs for KITTI3D and a single A100 GPU for Waymo during pre-training, with a total batch size of 16.

During fine-tuning, we initialize the encoder’s weights with the pre-trained context encoder’s weights and then fine-tune using detection models: SECOND [3], PVRCNN [33], and Centerpoint [32] (we use encoders without residual connections) for 80 epochs, with all default hyperparameter settings in the OpenPCDet framework. We compare models trained from scratch and the most recent SOTA self-supervised pre-training methods, Occupancy-MAE [1]

¹Moderate level of difficulty is defined in [35] and LEVEL 2 difficulty, mentioned later in the text, is defined in [36].

and ALSO [2]. Specifically, we reproduce Occupancy-MAE using their default settings to obtain the pre-trained weights and fine-tune the downstream object detector. For ALSO, we directly fine-tune the released pre-trained encoder weights for the downstream object detector. The comparison methods use the same fine-tuning settings as ours. For all fine-tuning experiments, we fine-tune the model through three independent runs and report the best performance, in the same manner as [16] reports their results. The reproduced results may vary from the original papers. We use 4 1080 Ti GPUs for KITTI3D and 4 RTX 4090 GPU for Waymo during fine-tuning, with a total batch size of 16.

C. Downstream fine-tuning performance

Method	Cars	Ped.	Cycl.	Overall	Diff.
SECOND (80 epoch) - R_{40} metric					
No pre-training	81.99	52.02	65.07	66.36	
Occupancy-MAE [1]	81.15	50.36	69.74	67.08	+0.72
ALSO [2]	81.48	52.50	65.95	66.64	+0.28
AD-L-JEPA (ours)	81.68	54.15	67.93	67.92	+1.56
SECOND (80 epoch) - R_{11} metric					
No pre-training	78.89	53.78	64.93	65.87	
Occupancy-MAE [1]	78.15	52.10	69.39	66.55	+0.68
ALSO [2]	78.37	53.94	66.06	66.12	+0.25
AD-L-JEPA (ours)	78.51	54.86	67.94	67.10	+1.23
PV-RCNN (80 epoch) - R_{40} metric					
No pre-training	84.65	56.19	72.19	71.01	
Occupancy-MAE [1]	84.34	57.55	71.33	71.07	+0.06
ALSO [2]	84.64	57.09	73.72	71.82	+0.81
AD-L-JEPA (ours)	85.07	59.68	73.02	72.59	+1.58
PV-RCNN (80 epoch) - R_{11} metric					
No pre-training	83.38	57.01	72.65	71.01	
Occupancy-MAE [1]	83.41	58.68	70.97	71.02	+0.01
ALSO [2]	83.48	57.99	72.89	71.45	+0.44
AD-L-JEPA (ours)	83.74	59.91	72.19	71.95	+0.94

TABLE I: 3D detection results on the KITTI3D validation set with moderate difficulty, reported with the AP (%) metric. The models are pre-trained with and fine-tuned on the KITTI3D data set.

masking ratio	0.25	0.5	0.75
mAP - R_{40}	66.21	67.92	67.24
mAP - R_{11}	65.73	67.10	66.76

TABLE II: Different masking ratio and the corresponding mAP (%) on KITTI3D data set with SECOND detection model.

Method	Veh.	Ped.	Cycl.	Overall	Diff.
Centerpoint (30 epoch) - AP metric					
No pre-training	63.28	63.95	66.78	64.67	
Occupancy-MAE [1]	63.20	64.20	67.20	64.87	+0.20
AD-L-JEPA (ours)	63.18	64.35	67.68	65.07	+0.40
Centerpoint (30 epoch) - APH metric					
No pre-training	62.77	57.98	65.55	62.10	
Occupancy-MAE [1]	62.70	58.29	66.00	62.33	+0.23
AD-L-JEPA (ours)	62.68	58.39	66.48	62.51	+0.41

TABLE III: 3D detection results on the Waymo validation set with LEVEL 2 difficulty and the AP (%) metric. The models are pre-trained with and fine-tuned on the Waymo 20% data set.

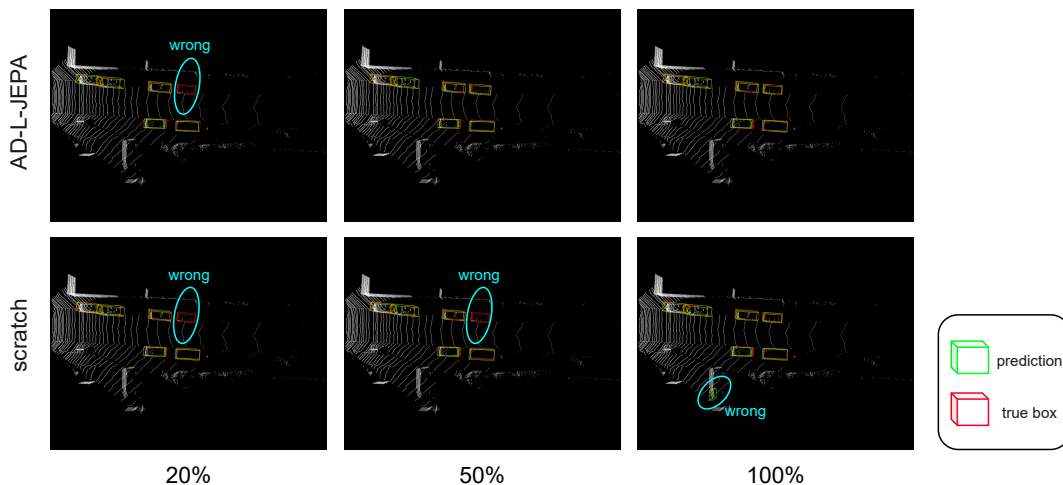


Fig. 4: Visual comparison of 3D object detection performance between SECOND trained from scratch and pre-trained with AD-L-JEPA, using 5%, 20%, and 100% of labeled data from the KITTI3D data set.

We first conduct self-supervised pre-training on KITTI3D without any labels and then fine-tune the network on the labeled training data from the same KITTI3D data set using the widely used SECOND [3] and PV-RCNN [33] methods. As shown quantitatively in Table I, our self-supervised pre-training approach significantly outperforms the baseline that corresponds to training from scratch and also surpasses other competitor algorithms. Table II presents ablation studies with different masking ratios during pre-training and their corresponding impact on downstream object detection performance for SECOND detection model and KITTI3D data set. We find that at a masking ratio of 0.5, the difficulty is moderate and yields the best performance; thus, we set 0.5 as the default masking ratio.

Next, in Table III we report the results of pre-training and fine-tuning with Waymo training data. The overall Average Precision across all classes outperforms the baseline trained from scratch, and our reproduced results using Occupancy-MAE. Notably, as the Waymo 20% data set is approximately 10 times larger than KITTI, pre-training takes considerably longer, and there is a significant difference in the pre-training speed between AD-L-JEPA and Occupancy-MAE. Unlike Occupancy-MAE, which is a generative method involving computationally expensive dense 3D convolutional layers to reconstruct invisible parts, AD-L-JEPA employs a joint-embedding predictive architecture at the BEV embedding level and does not require such layers. It takes about 12 hours to pre-train using Occupancy-MAE for the default three epochs on 4 A100 GPUs, totaling approximately 48 A100 GPU hours. In contrast, pre-training with AD-L-JEPA for 30 epochs on a single A100 GPU takes only 10 hours, which translates to a significant improvement in computational efficiency.

D. Transfer learning and label efficiency performance

In this section, we report the transfer learning capability when moving from Waymo 20% data set to KITTI3D with

Method	Cars	Ped.	Cycl.	Overall	Diff.
20%, SECOND - R_{40} metric					
No pre-training	79.11	44.36	62.55	62.01	
Occupancy-MAE [1]	79.04	43.85	63.46	62.12	+0.11
AD-L-JEPA (ours)	79.48	48.48	61.92	63.30	+1.29
20%, SECOND - R_{11} metric					
No pre-training	77.84	45.78	62.46	62.03	
Occupancy-MAE [1]	77.63	45.68	63.66	62.32	+0.29
AD-L-JEPA (ours)	78.11	49.71	62.18	63.33	+1.30
50%, SECOND - R_{40} metric					
No pre-training	81.05	48.75	62.83	64.21	
Occupancy-MAE [1]	81.20	48.17	63.80	64.49	+0.28
AD-L-JEPA (ours)	81.55	50.13	64.12	65.27	+1.06
50%, SECOND - R_{11} metric					
No pre-training	78.07	50.53	62.95	63.85	
Occupancy-MAE [1]	78.27	49.67	63.80	63.91	+0.06
AD-L-JEPA (ours)	78.38	52.04	63.53	64.65	+0.80
100%, SECOND - R_{40} metric					
No pre-training	81.99	52.02	65.07	66.36	
Occupancy-MAE [1]	81.65	51.51	66.72	66.63	+0.27
Occupancy-MAE [†] [1]	81.78	48.92	67.34	66.01	-0.35
AD-L-JEPA (ours)	81.83	52.41	66.73	66.99	+0.63
AD-L-JEPA [†] (ours)	80.92	52.45	69.76	67.71	+1.35
100%, SECOND - R_{11} metric					
No pre-training	78.89	53.78	64.93	65.87	
Occupancy-MAE [1]	78.47	52.60	67.23	66.10	+0.23
Occupancy-MAE [†] [1]	78.61	49.49	66.84	64.98	-0.89
AD-L-JEPA (ours)	78.65	53.62	67.12	66.46	+0.59
AD-L-JEPA [†] (ours)	77.90	54.01	69.30	67.07	+1.20

TABLE IV: Transfer learning experiment: pre-training on Waymo (20% of the data set) and fine-tuning on KITTI3D. We report 3D detection results on the KITTI3D validation set with moderate difficulty, with the AP (%) metric. Label efficiency is studied when fine-tuning with 20%, 50%, and 100% of the data. [†] denotes that the first layer of the model is randomly initialized.

AD-L-JEPA.

Each point in the Waymo 20% data set features five attributes: ['x', 'y', 'z', 'intensity', 'elongation'], whereas

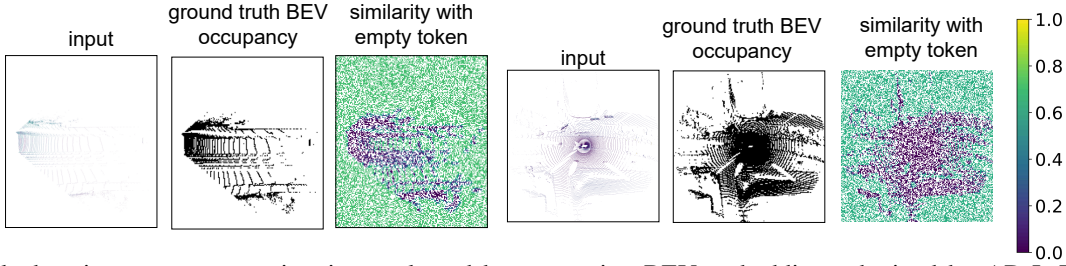


Fig. 5: Masked region occupancy estimation evaluated by comparing BEV embeddings obtained by AD-L-JEPA with the learnable empty token via the cosine similarity. Unmasked regions are ignored and the cosine similarity in this case is represented in white color.

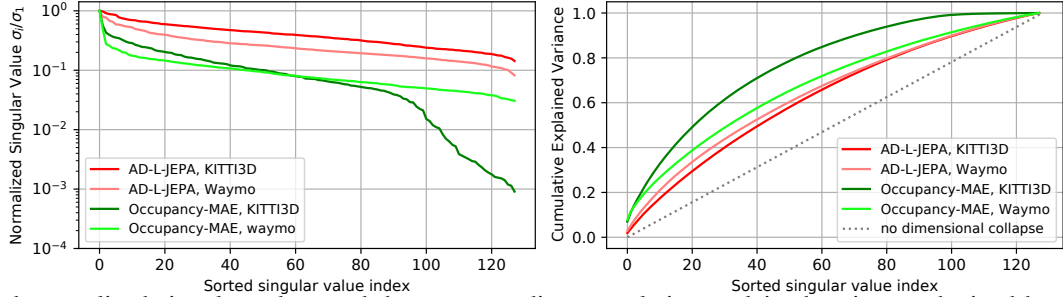


Fig. 6: Sorted normalized singular values and the corresponding cumulative explained variance, obtained by singular value decomposition of pre-trained BEV embeddings. Embeddings are obtained either with AD-L-JEPA or Occupancy-MAE.

each point in the KITT13D data set includes four attributes: $[x, y, z, \text{intensity}]$. Consequently, the first layer of the encoder pre-trained on the Waymo data set has a shape of $[5, 16, 3, 3, 3]$, while the first layer used for object detection on the KITT13D data set has a shape of $[4, 16, 3, 3, 3]$ to accommodate the respective point features with a sparse 3D convolutional kernel of 3. The remaining layers have the same shape in both the pre-trained and downstream networks. When fine-tuning the downstream network with an encoder pre-trained directly on the Waymo 20% data set without modifications, the first layer is randomly initialized, while the remaining layers of the 3D encoder retain the pre-trained weights. In the bottom of Table IV, models denoted by \dagger (Occupancy-MAE † and AD-L-JEPA † (ours)) present the quantitative results for this scenario using 100% of the fine-tuning data. Surprisingly, even though the first layer is randomly initialized, the downstream task still benefits from positive transfers in case of AD-L-JEPA, while Occupancy-MAE experiences negative transfers. This experiment demonstrates that even if not all encoder layers are initialized from pre-trained weights, the intermediate pre-trained layers of our method are robust and continue to benefit the downstream tasks.

Next, we modify the first layer of the encoder used for pre-training on the Waymo 20% data set to the shape of $[4, 16, 3, 3, 3]$ and redo the pre-training, utilizing only the first four features: $[x, y, z, \text{intensity}]$, while ignoring the fifth feature ‘elongation’. This adjustment allows all layers of the encoder used for the downstream KITT13D object detection task to be initialized from pre-trained weights. We also explore fine-tuning with varying amounts of labels. Specifically, we report fine-tuning with 20%, 50%, and 100% of the data and corresponding fine-tuning epochs of 320, 160,

and 80, respectively, to ensure the enough number of fine-tuning iterations. Figure 4 shows the qualitative comparisons with training from scratch. Table IV quantitatively shows that models using our pre-training method consistently perform the best across different label efficiencies. In the 100% setting specifically, models pre-trained with AD-L-JEPA † perform better. This improvement may be due to the fact that other layers, except for the first layer in the encoder, are pre-trained with the original 5-point features instead of modified 4-point features, which enables better representation learning with additional information.

E. Other evaluations

We also interpret the representation capability of AD-L-JEPA by the following method:

1) *Occupancy estimation*: In Figure 5, we estimate the occupancy of masked regions in the input point cloud at a downsampled BEV embedding resolution by comparing each grid’s BEV embeddings, outputted by our pre-trained model, against the learnable empty token using cosine similarity. The cosine similarity assigns high similarity to empty grids and low similarity to non-empty grids. We then compare the cosine similarity map with ground truth BEV occupancy side-by-side. Note that the similarity assigned to empty grids by our method is approximately 0.7, not 1, showcasing the model’s ability to represent the complex and highly uncertain nature of autonomous driving scenes.

2) *Singular value decomposition analysis*: We follow the methodology described in [23] to conduct singular value decomposition of non-empty BEV embeddings outputted by encoders pre-trained with AD-L-JEPA and Occupancy-MAE. This analysis assesses the level of dimensional collapse in pre-trained embeddings. Figure 6 shows that the normalized sorted singular values for AD-L-JEPA are more evenly

distributed, while the corresponding cumulative explained variance increases more slowly, indicating less dimensional collapse and less redundant information in the embeddings.

V. CONCLUSIONS

In this paper, we propose AD-L-JEPA, the first joint-embedding predictive architecture for self-supervised representation learning of autonomous driving LiDAR data. It learns a spatial world model in the BEV embedding space without any labeled data by learning. It does not require the manual creation of positive/negative pairs for contrastive learning, nor does it need to explicitly reconstruct the complex, high-uncertainty driving scenes. Extensive experiments show that AD-L-JEPA is a more efficient pre-training method compared to SOTA and learns faster better data representations that are useful for downstream task generalization. For the future work, we will extend AD-L-JEPA to utilize the temporal nature of autonomous driving scenarios and learn a spatial-temporal world models.

REFERENCES

- [1] C. Min, L. Xiao, D. Zhao, Y. Nie, and B. Dai, "Occupancy-mae: Self-supervised pre-training large-scale lidar point clouds with masked occupancy autoencoders," *IEEE Transactions on Intelligent Vehicles*, 2023.
- [2] A. Boulch, C. Sautier, B. Michele, G. Puy, and R. Marlet, "Also: Automotive lidar self-supervision by occupancy estimation," in *Proceedings of the IEEE/CVF Conference on Computer Vision and Pattern Recognition*, 2023, pp. 13 455–13 465.
- [3] Y. Yan, Y. Mao, and B. Li, "Second: Sparsely embedded convolutional detection," *Sensors*, vol. 18, no. 10, p. 3337, 2018.
- [4] Y. LeCun, "A path towards autonomous machine intelligence version 0.9. 2, 2022-06-27," *Open Review*, vol. 62, 2022.
- [5] S. Xie, J. Gu, D. Guo, C. R. Qi, L. Guibas, and O. Litany, "Pointcontrast: Unsupervised pre-training for 3d point cloud understanding," in *Computer Vision—ECCV 2020: 16th European Conference, Glasgow, UK, August 23–28, 2020, Proceedings, Part III 16*. Springer, 2020, pp. 574–591.
- [6] Z. Zhang, R. Girdhar, A. Joulin, and I. Misra, "Self-supervised pretraining of 3d features on any point-cloud," in *Proceedings of the IEEE/CVF International Conference on Computer Vision*, 2021, pp. 10 252–10 263.
- [7] J. Yin, D. Zhou, L. Zhang, J. Fang, C.-Z. Xu, J. Shen, and W. Wang, "Proposalcontrast: Unsupervised pre-training for lidar-based 3d object detection," in *European conference on computer vision*. Springer, 2022, pp. 17–33.
- [8] H. Liang, C. Jiang, D. Feng, X. Chen, H. Xu, X. Liang, W. Zhang, Z. Li, and L. Van Gool, "Exploring geometry-aware contrast and clustering harmonization for self-supervised 3d object detection," in *Proceedings of the IEEE/CVF International Conference on Computer Vision*, 2021, pp. 3293–3302.
- [9] S. Huang, Y. Xie, S.-C. Zhu, and Y. Zhu, "Spatio-temporal self-supervised representation learning for 3d point clouds," in *Proceedings of the IEEE/CVF International Conference on Computer Vision*, 2021, pp. 6535–6545.
- [10] L. Nunes, R. Marcuzzi, X. Chen, J. Behley, and C. Stachniss, "Seg-contrast: 3d point cloud feature representation learning through self-supervised segment discrimination," *IEEE Robotics and Automation Letters*, vol. 7, no. 2, pp. 2116–2123, 2022.
- [11] Y. Wu, T. Zhang, W. Ke, S. Süssstrunk, and M. Salzmann, "Spatiotemporal self-supervised learning for point clouds in the wild," in *Proceedings of the IEEE/CVF Conference on Computer Vision and Pattern Recognition*, 2023, pp. 5251–5260.
- [12] L. Nunes, L. Wiesmann, R. Marcuzzi, X. Chen, J. Behley, and C. Stachniss, "Temporal consistent 3d lidar representation learning for semantic perception in autonomous driving," in *Proceedings of the IEEE/CVF Conference on Computer Vision and Pattern Recognition*, 2023, pp. 5217–5228.
- [13] J. Yuan, B. Zhang, X. Yan, B. Shi, T. Chen, Y. Li, and Y. Qiao, "Ad-pt: Autonomous driving pre-training with large-scale point cloud dataset," *Advances in Neural Information Processing Systems*, vol. 36, 2024.
- [14] W. Wei, F. K. Nejadasl, T. Gevers, and M. R. Oswald, "T-mae: temporal masked autoencoders for point cloud representation learning," in *European Conference on Computer Vision*. Springer, 2025, pp. 178–195.
- [15] D. Hegde, S. Lohit, K.-C. Peng, M. J. Jones, and V. M. Patel, "Equivariant spatio-temporal self-supervision for lidar object detection," in *European Conference on Computer Vision*. Springer, 2025, pp. 475–491.
- [16] C. Sautier, G. Puy, A. Boulch, R. Marlet, and V. Lepetit, "Bevcontrast: Self-supervision in bev space for automotive lidar point clouds," in *2024 International Conference on 3D Vision (3DV)*. IEEE, 2024, pp. 559–568.
- [17] Z. Lin, Y. Wang, S. Qi, N. Dong, and M.-H. Yang, "Bev-mae: Bird's eye view masked autoencoders for point cloud pre-training in autonomous driving scenarios," in *Proceedings of the AAAI Conference on Artificial Intelligence*, vol. 38, 2024, pp. 3531–3539.
- [18] R. Xu, T. Wang, W. Zhang, R. Chen, J. Cao, J. Pang, and D. Lin, "Mv-jar: Masked voxel jigsaw and reconstruction for lidar-based self-supervised pre-training," in *Proceedings of the IEEE/CVF Conference on Computer Vision and Pattern Recognition*, 2023, pp. 13 445–13 454.
- [19] B. Agro, Q. Sykora, S. Casas, T. Gilles, and R. Urtasun, "Uno: Unsupervised occupancy fields for perception and forecasting," in *Proceedings of the IEEE/CVF Conference on Computer Vision and Pattern Recognition*, 2024, pp. 14 487–14 496.
- [20] M. Assran, Q. Duval, I. Misra, P. Bojanowski, P. Vincent, M. Rabbat, Y. LeCun, and N. Ballas, "Self-supervised learning from images with a joint-embedding predictive architecture," in *Proceedings of the IEEE/CVF Conference on Computer Vision and Pattern Recognition*, 2023, pp. 15 619–15 629.
- [21] A. Bardes, Q. Garrido, J. Ponce, X. Chen, M. Rabbat, Y. LeCun, M. Assran, and N. Ballas, "Revisiting feature prediction for learning visual representations from video," *arXiv preprint arXiv:2404.08471*, 2024.
- [22] A. Bardes, J. Ponce, and Y. LeCun, "Vicreg: Variance-invariance-covariance regularization for self-supervised learning," in *ICLR*, 2022.
- [23] A. C. Li, A. A. Efros, and D. Pathak, "Understanding collapse in non-contrastive siamese representation learning," in *European Conference on Computer Vision*. Springer, 2022, pp. 490–505.
- [24] D. Ha and J. Schmidhuber, "Recurrent world models facilitate policy evolution," *Advances in neural information processing systems*, vol. 31, 2018.
- [25] A. Fu, Y. Zhou, T. Zhou, Y. Yang, B. Gao, Q. Li, G. Wu, and L. Shao, "Exploring the interplay between video generation and world models in autonomous driving: A survey," *arXiv preprint arXiv:2411.02914*, 2024.
- [26] A. Hu, L. Russell, H. Yeo, Z. Murez, G. Fedoseev, A. Kendall, J. Shotton, and G. Corrado, "Gaia-1: A generative world model for autonomous driving," *arXiv preprint arXiv:2309.17080*, 2023.
- [27] A. Popov, A. Degirmenci, D. Wehr, S. Hegde, R. Oldja, A. Kamenev, B. Douillard, D. Nistér, U. Müller, R. Bhargava, et al., "Mitigating covariate shift in imitation learning for autonomous vehicles using latent space generative world models," *arXiv preprint arXiv:2409.16663*, 2024.
- [28] Y. Li, L. Fan, J. He, Y. Wang, Y. Chen, Z. Zhang, and T. Tan, "Enhancing end-to-end autonomous driving with latent world model," *arXiv preprint arXiv:2406.08481*, 2024.
- [29] P. Li and D. Cui, "Does end-to-end autonomous driving really need perception tasks?" *arXiv preprint arXiv:2409.18341*, 2024.
- [30] Z. Yang, L. Chen, Y. Sun, and H. Li, "Visual point cloud forecasting enables scalable autonomous driving," in *Proceedings of the IEEE/CVF Conference on Computer Vision and Pattern Recognition*, 2024, pp. 14 673–14 684.
- [31] S. Shi, X. Wang, and H. Li, "Pointcnn: 3d object proposal generation and detection from point cloud," in *Proceedings of the IEEE/CVF conference on computer vision and pattern recognition*, 2019, pp. 770–779.
- [32] T. Yin, X. Zhou, and P. Krahenbuhl, "Center-based 3d object detection and tracking," in *Proceedings of the IEEE/CVF conference on computer vision and pattern recognition*, 2021, pp. 11 784–11 793.
- [33] S. Shi, C. Guo, L. Jiang, Z. Wang, J. Shi, X. Wang, and H. Li, "Pv-rcnn: Point-voxel feature set abstraction for 3d object detection,"

in *Proceedings of the IEEE/CVF conference on computer vision and pattern recognition*, 2020, pp. 10 529–10 538.

- [34] O. D. Team, “Openpcdet: An open-source toolbox for 3d object detection from point clouds,” <https://github.com/open-mmlab/OpenPCDet>, 2020.
- [35] A. Geiger, P. Lenz, and R. Urtasun, “Are we ready for autonomous driving? the kitti vision benchmark suite,” in *2012 IEEE conference on computer vision and pattern recognition*. IEEE, 2012, pp. 3354–3361.
- [36] P. Sun, H. Kretschmar, X. Dotiwalla, A. Chouard, V. Patnaik, P. Tsui, J. Guo, Y. Zhou, Y. Chai, B. Caine, *et al.*, “Scalability in perception for autonomous driving: Waymo open dataset,” in *Proceedings of the IEEE/CVF conference on computer vision and pattern recognition*, 2020, pp. 2446–2454.